



DØ-CONF-6463

A Precise Measurement of the Top Quark Mass in Dilepton Events with the DØ Detector

The DØ Collaboration

URL <http://www-d0.fnal.gov>

(Dated: May 7, 2015)

We present a measurement of the top quark mass in dilepton final states of $t\bar{t}$ events in $p\bar{p}$ collisions at $\sqrt{s} = 1.96$ TeV, using the full DØ Run II data corresponding to an integrated luminosity of 9.7 fb^{-1} at the Fermilab Tevatron. We extract the top quark mass by reconstructing event kinematics, and integrating over expected neutrino rapidity distributions to obtain solutions over a scanned range of top quark mass hypotheses. The analysis features a comprehensive optimization to minimize the expected statistical uncertainty. We also improve the calibration of jets in dilepton events by using the calibration determined in $t\bar{t} \rightarrow \text{lepton} + \text{jets}$ events, which reduces the otherwise limiting systematic uncertainty from the jet energy scale. The measured mass is $173.3 \pm 1.4(\text{stat}) \pm 0.5(\text{JES}) \pm 0.7(\text{sys}) \text{ GeV} = 173.3 \pm 1.6 \text{ GeV}$.

Preliminary Results for Spring Conferences

I. INTRODUCTION

The standard model (SM) of quantum chromodynamics (QCD) and electroweak interactions involves three generations of leptons and quarks, several mediating gauge vector bosons, and one scalar Higgs boson. The top quark stands out because of its large mass. Its Yukawa coupling to the Higgs boson, $Y_t = \sqrt{2}m_t/v$, where v is the vacuum expectation, is of order unity. The precise measurement of m_t will provide a strong test of the linear relationship between fermion Yukawa coupling and mass in the SM once the LHC experiments deliver direct measurements of Y_t . In addition, m_t is linked to the W and Higgs boson masses, M_W and M_H , via one-loop radiative corrections to M_W . Following the Higgs boson discovery [1, 2], precise measurement of m_t facilitates a strong test of the electroweak model and provides information on whether our universe resides in a stable or metastable region of that theory [3]. The short lifetime of the top quark prevents its confinement in the strong color field since top quarks tend to decay before hadronization. The mass of the top quark provides a valuable probe of higher order QCD contributions via comparison of the measured m_t and determinations of the pole mass [4].

Assuming the SM branching ratio of $t \rightarrow Wb \approx 100\%$, $t\bar{t}$ decay yields three distinct final state categories according to whether they have 0, 1 or 2 high p_T leptons from W boson decays. Dilepton (2ℓ) events are relatively rare but have low background. Lacking a dijet signature from $W \rightarrow q\bar{q}'$ for calibration, previous 2ℓ analyses at the Tevatron have reached the sensitivity limit imposed by standard jet calibration methods [5, 6]. Progress in calibrating jets in the 2ℓ channel [7] can provide improved cross checks across different channels and a more sensitive contribution from 2ℓ channels to the average m_t [8, 9].

We present a measurement of m_t with $p\bar{p}$ collider data collected with the D0 detector, corresponding to an integrated luminosity of 9.7 fb^{-1} , in events with two leptons, electrons or muons, with large transverse momenta (p_T). Two high p_T jets must also be observed, one of which must be consistent with a b quark. In this analysis, we optimized the method to maximize statistical sensitivity and substantially reduced the systematic uncertainties. Based on an optimization of the operating parameters of this method, we minimize the substantial statistical contributions to the uncertainties of the analysis. We control an otherwise dominant jet energy scale uncertainty using the methods of Ref. [7].

II. DETECTOR AND DATA SAMPLE

A. Detector

The D0 detector [10] has a central-tracking system, consisting of a silicon microstrip tracker and a central fiber tracker, both located within a 1.9 T superconducting solenoidal magnet, with designs optimized for tracking and vertexing at pseudorapidities [11] $|\eta| < 3$ and $|\eta| < 2.5$, respectively. A liquid-argon and uranium calorimeter has a central section covering $|\eta|$ up to ≈ 1.1 , and two end calorimeters that extend coverage to $|\eta| \approx 4.2$, with all three housed in separate cryostats. An outer muon system, covering $|\eta| < 2$, consists of a layer of tracking detectors and scintillation trigger counters in front of 1.8 T toroids, followed by two similar layers after the toroids.

B. Event Reconstruction

We reconstruct the data to obtain momenta of charged hadrons and muons, and energies of electrons and jets. Charged leptons must have their extrapolated track trajectories isolated from significant additional calorimeter energy. We require electrons to satisfy an identification criterion based on Boosted Decision Trees [12] using calorimeter and tracking information. Muons must satisfy requirements on wire and scintillator hits in the muon system matching to a track in the central-tracking detector, which is required to have a small distance of closest approach to the beam axis [13]. We require hits in the muon layers inside and outside the toroid. Muons must be isolated from jets and nearby tracks adding to significant momenta. The electrons and muons must have $p_T > 15 \text{ GeV}$, and $|\eta| < 2.5$ or $|\eta| < 2.0$, respectively. We reconstruct jets using an iterative, midpoint cone algorithm with radius $\mathcal{R}_{\text{cone}} = \sqrt{\Delta\phi^2 + \Delta\eta^2} = 0.5$ [14]. We confirm jet identification in the independent hardware trigger readout. Muons embedded in jets incur an additional correction to jet energy to account for their associated neutrino. Jets are identified as originating from the hadronization of a hadron containing a b quark via a multivariate discriminant [15]. We define the event missing transverse momentum (\cancel{E}_T), originating from the neutrinos from two $W \rightarrow l\nu$ decays in $t\bar{t}$ events, to be opposite of the vector sum of all transverse components of calorimeter cell energies ($E \sin \theta$). We correct this for measured muon track momenta and the response of the calorimeter to electrons. Details of the object reconstruction are provided in Ref. [16].

C. Jet Energy Calibration

We calibrate jet energies reconstructed in the detector to the energies of matching particle jets [17]. Particle jets are reconstructed using the same cone algorithm applied to hadronization products before they interact in the detector. Jet energies are primarily affected by the response of the calorimeter to the constituent particles. Charged hadrons, in particular, have an energy dependent scale that is lower than electrons and photons, such that the electromagnetic to hadronic response $e/h > 1$. We apply corrections from γ +jet events to account for the net energy dependence of jet response in the central $|\eta|$ region. We also apply a relative correction dependent on the η of the jets that is obtained from γ +jet and dijet events. We employ the same methods to calibrate jets independently in the Monte Carlo (MC) simulation and data to ensure agreement of these two energy calibrations. We incorporate a correction for jets in the MC simulation that accounts for the difference in single particle response between data and MC. This procedure ensures that the flavor dependence of the jet response in data is replicated in MC. Other corrections are also applied to account for multiple $p\bar{p}$ interactions and to return to the full energy of only those particles directed within the jet cone at particle level. We correct event \cancel{E}_T for effects in jet energy calibration (e.g., e/h) that lead to undetected energy. The typical systematic uncertainty in the energy of each jet in the 2ℓ sample is 2%. This precision is limited by γ +jet systematic uncertainties in the p_T range of jets in $t\bar{t}$ events. Details about this calibration can be found in Ref. [17]. We require that the jets after calibration have $p_T > 20$ GeV and $|\eta| < 2.5$.

III. EVENT SELECTION

Events are required to pass single lepton triggers in the ee and $\mu\mu$ channels. No explicit trigger requirement is applied in the $e\mu$ channel. The nominal dilepton event selection is described in Ref. [16]. We then optimize the selection to provide the smallest expected statistical uncertainty in m_t . For all events, we require two isolated leptons with opposite electric charge. We require at least two jets in the events. At least one of the two jets with highest p_T must be identified as a b jet using a multivariate discriminant which yields an efficiency of 72% and light quark mis-tag rate of 12% in the central region for $e\mu$, and a few per cent lower efficiency and 30% lower mis-tag rate for the same-flavor channels (see Ref. [15]). We require events in the $\mu\mu$ channel to have $\cancel{E}_T > 40$ GeV. This selection is also applied to ee events but only when the dilepton invariant mass is between 70 GeV and 100 GeV to decrease the $Z \rightarrow ee$ background contribution. Additionally, the same-flavor 2ℓ channels must satisfy a \cancel{E}_T discriminant involving a likelihood test that can be interpreted as the number of standard deviations (σ) for the measured \cancel{E}_T to differ from 0. The ee and $\mu\mu$ channels must have discriminant values corresponding to at least 3.5 and 4 σ , respectively. We require $e\mu$ events to have $H_T > 100$ GeV, where H_T is defined as the scalar sum of the p_T of the two leading jets and the lepton with highest p_T . The \cancel{E}_T , H_T and b -tag requirements are optimized to minimize the expected statistical uncertainty in each channel. The expected signal-to-background ratio (S/B) is about 7 for these channels. This yields a 3% improvement in the m_t statistical precision relative to the nominal selection. After the selection, we obtain 340, 115 and 110 events in the $e\mu$, ee and $\mu\mu$ channels, respectively.

IV. MODELING SIGNAL AND BACKGROUND

The $t\bar{t}$ events are simulated at 15 mass points over the range $130 \leq m_t^{MC} \leq 200$ GeV using the leading-order (LO) ALPGEN 2.11 generator [18] and PYTHIA 6.409 [19] for parton showering and hadronization. Here, m_t^{MC} refers to the input mass at the $t\bar{t}$ generator level. An additional, higher statistics sample is generated at $m_t^{MC} = 172.5$ GeV to study systematic uncertainties. We use a $t\bar{t}$ cross section of 7.24 pb [20], which is calculated to next-to-next-to-leading order with next-to-next-to-leading logarithm soft gluon resummation. The main backgrounds arise from three sources: Z/γ^* and diboson ($WW, WZ, ZZ \rightarrow 2\ell$) process, and instrumental effects. We model the former with ALPGEN interfaced to PYTHIA, while we employ PYTHIA for the diboson background. The instrumental background arises from W +jets or multijet production where one or two jets are either mistaken as electrons, or where they contain a hadron decaying to a non-isolated lepton that passes our selection. This background is estimated from data as in Ref. [16]. We use a full detector simulation based on GEANT 3.14 [21] for all generated events. The expected sums of $t\bar{t}$ and background yields are 298.1 ± 4.4 (stat) $^{+21.7}_{-26.8}$ (syst), 106.5 ± 1.9 (stat) $^{+10.2}_{-11.4}$ (syst) and 103.5 ± 0.8 (stat) $^{+7.4}_{-9.1}$ (syst) events for the $e\mu$, ee and $\mu\mu$ channels, respectively.

V. ABSOLUTE JET CALIBRATION FROM A $W \rightarrow q\bar{q}'$ CONSTRAINT

As in Ref. [7], we apply a correction to the absolute normalization of the jet energy scale from the analysis of 9.7 fb^{-1} of ℓ +jets events. The dijet mass from the $W \rightarrow q\bar{q}'$ decays provides a constraint of $1.0250 \pm 0.0046(\text{stat})$ [22]. We apply this correction and uncertainty to jets in data to improve agreement of data with the MC. This reduces the uncertainty on the absolute scale by a factor of about four relative to the standard jet energy scale, while retaining the η and p_T dependence of the standard correction. The mass measurement requires agreement between data and MC within a given event topology. Since our current standard jet energy scale [17] uses single particle responses to correct for data-to-MC differences on a jet-by-jet basis, we ensure that b jets in 2ℓ simulated samples look like b jets in the 2ℓ data sample. Therefore, we apply the ℓ +jets absolute scale as a calibration.

VI. KINEMATIC RECONSTRUCTION

A. Neutrino Weighting

Due to the presence of two neutrinos in the $t\bar{t}$ event, there are insufficient kinematic constraints to extract a unique m_t measurement from each event. Given the measured leptons, jets and \cancel{E}_T , and available SM constraints from the W boson mass and $m_t = m_{\bar{t}}$, 2ℓ events require one additional constraint to provide a full $t\bar{t}$ reconstruction. To address this challenge, we integrate over the phase space of neutrino rapidities for chosen values of fixed m_t [23]. For each event at a hypothesized m_t , each chosen point of phase space provides solutions of the neutrino momenta. We compare their vector sum to the observed \cancel{E}_T to determine a level of consistency, or “weight”, within the \cancel{E}_T resolution:

$$\omega = \frac{1}{N_{\text{iter}}} \sum_{i=1}^{N_{\text{iter}}} \exp\left(\frac{-(\cancel{E}_{x,i}^{\text{calc}} - \cancel{E}_x^{\text{obs}})^2}{2\sigma_{\cancel{E}_x}^2}\right) \exp\left(\frac{-(\cancel{E}_{y,i}^{\text{calc}} - \cancel{E}_y^{\text{obs}})^2}{2\sigma_{\cancel{E}_y}^2}\right). \quad (1)$$

All combinatoric configurations with real quadratic neutrino solutions and any association of each of the leading two jets to a lepton are summed. Doing this for a range of m_t yields a distribution of weight vs. m_t . Prior studies [24] show that the first two moments (μ_w, σ_w) of this distribution extract most of the information about m_t .

B. Optimization of Weight Calculation Parameters

Given the improvements in jet energy calibration, the statistical contribution becomes the dominant source of uncertainty in the 2ℓ channel. We therefore examine all parameters for the kinematic reconstruction of $t\bar{t}$ events, and for the maximum likelihood fit described below, to provide a reduction in expected statistical uncertainty. At each step, we verify that the optimization does not increase the systematic uncertainty. A critical element of the analysis concerns the range of m_t scanned in the weight distribution. Although all neutrino solutions and jet assignments yield mass estimators such as μ_w that are correlated with m_t , the correlation is substantially greater and μ_w values are less biased when the correct jet assignments and solutions are chosen. Considering a very wide range in m_t causes the incorrect configurations to overwhelm the correct contribution, thereby worsening the mass resolution. Likewise, scanning over too narrow of a range biases the background and worsens the mass sensitivity by making $t\bar{t}$ and backgrounds look similar. Examination of a two dimensional grid of upper and lower choices of limit yields the optimal mass range of 115 GeV to 220 GeV for an assumed $m_t = 172.5$ GeV. The unclustered \cancel{E}_T ($\cancel{E}_T^{\text{unc}}$) is the magnitude of the vector sum of all energy deposits in the calorimeter that were not included in the lepton or jet reconstruction. The resolution in $\cancel{E}_T^{\text{unc}}$ links the neutrino momentum solutions with the measured \cancel{E}_T in the weight calculation. We measured this resolution as a function of the unclustered scalar E_T in data and in MC $Z \rightarrow \ell\ell$ +jets events, and found them to agree. To account for the full difference between calculated and measured \cancel{E}_T , including effects such as mismatches in neutrino p_T from finite binning of the neutrino rapidity distributions, we optimized the value of the \cancel{E}_T resolution parameter. Combined, these optimizations improve the expected statistical uncertainty on m_t by 11% compared to the nominal parameters used in Ref. [7]. The kinematic reconstruction efficiency is over 99% for $t\bar{t}$ and 91% to 98% for the backgrounds. Events passing kinematic reconstruction total 336, 113 and 109 events in the $e\mu$, ee and $\mu\mu$ channels, respectively. The distributions of μ_w before and after applying selections on the optimization variables (b -tag, \cancel{E}_T , \cancel{E}_T significance and H_T) are shown in Fig 1. Evidence of a $t\bar{t}$ is evident in the background enriched sample. The mass dependence of the μ_w distribution is shown in the signal sample.

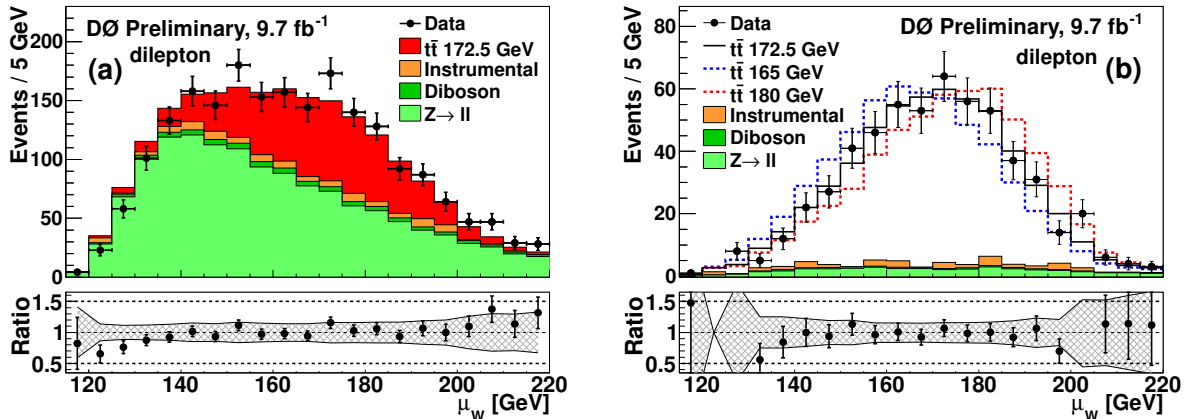


FIG. 1. The distribution in the means of event weights, μ_w , for the combination of ee , $e\mu$, and $\mu\mu$ channels before (a) and after (b) the event selection using b -tagging, \cancel{E}_T , \cancel{E}_T significance and H_T optimization variables. The MC events are normalized separately to the number of observed events in data in each channel. The distributions in μ_w for input $m_t = 172.5$ GeV, 165 GeV and 180 GeV in the combined ee , $e\mu$, and $\mu\mu$ channels are compared in (b). The ratio shows the number of observed events divided by the number of expected events in a given bin of μ_w . The band of systematic uncertainty includes contributions from dominant sources: jet energy scale, lepton identification, lepton momentum scale, luminosity, b quark modeling, initial and final state radiation, color reconnection, as well as hadronization and higher-order effects for $t\bar{t}$ events.

VII. EXTRACTING THE TOP QUARK MASS

A. Maximum Likelihood

We perform a binned maximum likelihood fit to the extracted distribution of moments $[\mu_w, \sigma_w]$ in data. Expected probability densities are calculated for each of the 16 m_t mass points, yielding a two dimensional probability density $h_s(\mu_w, \sigma_w | m_t^{MC})$ distribution parametrized by m_t . Background samples are used to construct a background template for each channel, $h_b(\mu_w, \sigma_w)$, with each background contributing according to its expected yield. Bins with no events are given a weighted value expected for a single MC event. The binning of the templates is optimized in a two dimensional grid allowing μ_w and σ_w bin sizes to vary over a wide range. Using pseudo-experiments, this yields a 10% improvement in statistical precision on m_t . The likelihood is given by:

$$\mathcal{L}(\mu_w\{1..N\}, \sigma_w\{1..N\}, N | n_s, n_b, m_t) = \prod_{i=1}^N \frac{n_s h_s(\mu_{w_i}, \sigma_{w_i} | m_t) + n_b h_b(\mu_{w_i}, \sigma_{w_i})}{n_s + n_b}, \quad (2)$$

where N is the number of observed events, n_s is the number of expected $t\bar{t}$ events (for $m_t = 172.5$ GeV) and n_b is the expected number of total background. We fit $-\ln \mathcal{L}$ vs. m_t^{MC} to a parabola, iterated to yield a stable minimum. We fit in a window around the minimum that has been optimized to be 15 GeV, which yields a small improvement in the $\mu\mu$ statistical precision. We take the minimum of this parabola to be the fitted top quark mass m_t^{fit} . The uncertainty on the most likely m_t^{MC} is obtained by considering the mass range where the fit function rises by 0.5 units in $-\ln \mathcal{L}$ above this minimum. The optimization of the maximum likelihood fit improves the expected statistical uncertainty by $> 10\%$ relative to the nominal parameters in Ref. [7]. Overall, optimizations in this analysis have improved statistical sensitivity by 25% beyond the gains obtained from the doubling of integrated luminosity.

B. Ensemble Testing and Data Results

We check the relationship between m_t^{fit} and the input m_t by performing pseudo-experiments using all signal mass points to obtain a linear relation between m_t^{fit} and m_t^{MC} . The events from the MC samples are randomly placed into pseudo-experiments according to MC weights. The number of signal and background events is allowed to fluctuate within their Poisson uncertainties around their expected values. We require that the total number of events matches that observed in the data. To minimize the impact of statistical fluctuations on our systematic uncertainties, we optimize the number of pseudo-experiments by dividing the MC sample into five subsamples, and measure most systematic uncertainties with each subsample. We calculate the RMS of the five uncertainties, average over all

TABLE I. Slopes, offsets and pull widths used to calibrate the fitted m_t and expected statistical uncertainties in the mass (σ_{m_t}) for the ee , $e\mu$, and $\mu\mu$ channels and their 2ℓ combination.

Ch.	Slope	Offset [GeV]	Pull width	σ_{m_t} [GeV]
ee	0.984 ± 0.004	0.672 ± 0.038	0.994	2.98
$e\mu$	0.985 ± 0.006	0.549 ± 0.064	0.998	1.72
$\mu\mu$	0.989 ± 0.010	0.718 ± 0.100	1.005	3.31
2ℓ	0.988 ± 0.006	0.617 ± 0.062	0.995	1.35

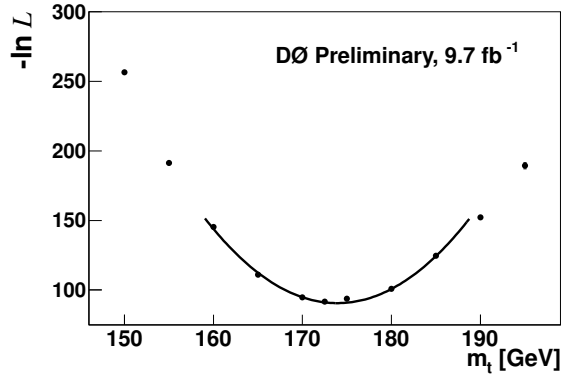


FIG. 2. The $-\ln \mathcal{L}$ as a function of m_t^{MC} for the combination of ee , $e\mu$, and $\mu\mu$ channels before calibration. A parabolic fit is shown within ± 15 GeV of the minimum value in m_t .

systematic effects, and divide by $\sqrt{4}$ to estimate the statistical component of our systematic uncertainties. The average RMS decreases until we oversample, or reuse, the $t\bar{t}$ MC events roughly three times. This corresponds to 3000 pseudo-experiments with the full MC samples. We linearly fit m_t^{fit} vs. m_t^{MC} to obtain a calibration slope and offset for m_t^{fit} where the origin is at $m_t = 170$ GeV. We increase the statistical uncertainties in each mass point by the oversampling factor appropriate to each. Likewise, we compute the pull width as the ratio of the average estimated uncertainty over the RMS of $m_t^{\text{fit}} - m_t^{MC}$ at each mass point. In general, the slope of m_t^{fit} vs. m_t^{MC} is close to 1.0, offsets are small, and pull widths are consistent with unity, as shown in Table I. We calculate the final m_t by correcting m_t^{fit} from a given measurement by the slope and offset. We correct the statistical uncertainty by the slope and the pull width. The expected corrected statistical uncertainties for each channel are given in Table I. In data, we obtain corrected, fitted m_t values of $171.9 \pm 1.7(\text{stat})$, $174.0 \pm 3.0(\text{stat})$ and $178.6 \pm 3.6(\text{stat})$ GeV for the $e\mu$, ee and $\mu\mu$ channels, respectively, and $173.3 \pm 1.4(\text{stat})$ GeV for the combined 2ℓ channel. The 2ℓ result is shown in Fig. 2.

VIII. SYSTEMATIC UNCERTAINTIES

Systematic uncertainties arise from jet energy calibration, $t\bar{t}$ and background modeling, object reconstruction, and the mass extraction method. The energies of jets are shifted up and down by the statistical uncertainty on the absolute energy scale taken from ℓ +jets events, providing thereby shifts in m_t . This scale is appropriate to light-quark jets whose kinematic distributions are different from those for b jets from $t\bar{t}$. The systematic uncertainty on the standard jet energy scale quantifies the range of potential dependences of energy scale on jet energy and η . We calculate a residual uncertainty due to the kinematic differences between the ℓ +jets calibration sample and 2ℓ sample of b jets. We use separate up and down estimates to extract the uncertainty. We cross-check this with the method applied to b jets in the ℓ +jets channel [22]. These methods agree, further validating the use of the ℓ +jets scale as a jet calibration. To estimate the uncertainty corresponding to possible variations of the MC scale's flavor dependence relative to data, we vary the flavor uncertainties up and down by one standard deviation and obtain the shift in m_t . For possible variation of the MC b quark fragmentation, we replace the PYTHIA b quark fragmentation function with the Bowler scheme [25], where the Bowler free parameters are tuned to LEP (ALEPH, OPAL, and DELPHI) and SLD data [26].

We evaluate the uncertainty associated with the modeling of initial and final state radiation by comparing ALPGEN+PYTHIA with the renormalization scale in the CKKW scale-setting procedure in ALPGEN varied up and down by

TABLE II. Systematic uncertainties on m_t for the combined dilepton measurement in 9.7 fb^{-1} of data.

Source	σ_{m_t} [GeV]
Jet energy calibration	
Absolute scale	± 0.5
Flavor dependence	± 0.3
Residual scale	± 0.4
<i>b</i> quark fragmentation	-0.1
Signal modeling	
ISR/FSR	± 0.2
Color reconnection	$+0.2$
Higher order effects	$+0.3$
Hadronization	$+0.1$
PDF uncertainty	± 0.1
Signal fraction	< 0.05
Object reconstruction	
Electron p_T resolution	< 0.05
Muon p_T resolution	< 0.05
Electron energy scale	< 0.05
Muon p_T scale	< 0.05
Jet resolution	± 0.1
Jet identification	< 0.05
Method	
Calibration	± 0.1
Template statistics	± 0.2

a factor of 1.5 [22]. We evaluate the effect of color reconnection by comparing m_t measurements in ALPGEN+PYTHIA samples with two different PYTHIA tunes: the Perugia2011 tune that incorporates an explicit color reconnection scheme, and the Perugia2011 NOCR tune that does not [27]. Higher order contributions are omitted in the LO ALPGEN of our standard $t\bar{t}$ simulation. We therefore compare our ensembles using MC@NLO 3.4 [28] $t\bar{t}$ events with ALPGEN events, where both employ HERWIG 6.510 [29] for modeling of hadronization. Since the hadronization in our default $t\bar{t}$ sample is modeled with PYTHIA, we estimate a hadronization uncertainty on m_t by performing pseudo-experiments using an ALPGEN+HERWIG sample. The uncertainty in the proton structure is obtained from the 20 sets of CTEQ6L1 parton distribution functions (PDFs) reweighted to CTEQ6M, where the deviations for the 20 sets are added in quadrature. We estimate the effect of uncertainty on the signal fraction by varying the expected $t\bar{t}$ event yields (n_s) up and down within its theoretical uncertainty.

The MC objects are smeared in energy to ensure that their resolutions reflect those in data. The uncertainties in these parameters for electron and jet energies, and muon momenta, are applied independently to object resolutions and the shifts in m_t are extracted as uncertainties. Lepton energy or momentum scales and uncertainties are extracted from $Z \rightarrow 2\ell$ events in data. An additional uncertainty is estimated for jet identification, where scale factors in the efficiencies are employed to obtain better agreement between data and MC. The jet identification efficiencies are shifted by their uncertainties in the MC samples to estimate their impact on m_t .

Our method of m_t extraction relies on the correction of the fitted m_t to the input MC mass. The uncertainties from this calibration are applied to provide the uncertainty in m_t . Our templates are constructed from MC samples for $t\bar{t}$, $Z \rightarrow 2\ell$ background and diboson background, and from data samples for instrumental background, yielding finite statistical uncertainties on their bin contents. We randomly modify our bin contents within their statistical uncertainties to obtain 1000 new templates. We measure m_t with these templates and the RMS of the measured mass is taken as an uncertainty. All systematic uncertainties are provided in Table II.

IX. CONCLUSION

We extract a measurement of m_t via a simultaneous fit to events across all dilepton channels, which yields a combined result of

$$173.3 \pm 1.4(\text{stat.}) \pm 0.8(\text{syst.}) \text{ GeV} = 173.3 \pm 1.6 \text{ GeV}. \quad (3)$$

This value is consistent with the current average [8] value of m_t . Our measurement is the most precise 2ℓ result from the Tevatron, and is competitive with the best LHC dilepton measurements. The systematic uncertainty of 0.5% is the lowest among all 2ℓ measurements.

We thank the staffs at Fermilab and collaborating institutions, and acknowledge support from the DOE and NSF (USA); CEA and CNRS/IN2P3 (France); MON, NRC KI, and RFBR (Russia); CNPq and FAPERJ (Brazil); DAE and DST (India); Colciencias (Colombia); CONACyT (Mexico); NRF (Korea); FOM (The Netherlands); STFC and The Royal Society (UK); MSMT (Czech Republic); BMBF and DFG (Germany); SFI (Ireland); Swedish Research Council (Sweden); CAS and CNSF (China); and MESU (Ukraine).

-
- [1] G. Aad *et al.* (ATLAS Collab.), Phys. Lett. B **716**, 1 (2012).
 - [2] S. Chatrchyan *et al.* (CMS Collab.), Phys. Lett. B **716**, 30 (2012).
 - [3] G. Degross *et al.*, J. High Energy Phys. **08**, 098 (2012).
 - [4] F. Jegerlehner, M. Kalmykov, B. Kniehl, Phys. Lett. B **722**, 123 (2013).
 - [5] V. Abazov *et al.* (D0 Collab.), Phys. Rev. Lett. **107**, 082004 (2011).
 - [6] T. Aaltonen *et al.* (CDF Collab.), Phys. Rev. D **83**, 111101 (2011).
 - [7] V. Abazov *et al.* (D0 Collab.), Phys. Rev. D **86**, 051103(R) (2012).
 - [8] ATLAS and CDF and CMS and D0 Collaborations, arXiv:1403.4427 (2014).
 - [9] CDF and D0 Collaborations, arXiv:1407.2682 (2014).
 - [10] V. Abazov *et al.* (D0 Collab.), Nucl. Instrum. Methods in Phys. Res. Sect. A **565**, 463 (2006).
 - [11] The pseudorapidity is defined as $\eta = -\ln[\tan(\theta/2)]$ where θ is the polar angle relative to the beam axis, defined relative to the center of the detector.
 - [12] V. Abazov *et al.* (D0 Collab.), Nucl. Instrum. Methods A **750**, 78 (2014).
 - [13] V. Abazov *et al.* (D0 Collab.), Nucl. Instrum. Methods A **737**, 281 (2014).
 - [14] G. Blazey *et al.*, arXiv:hep-ex/0005012 (2000).
 - [15] V. Abazov *et al.* (D0 Collab.), Nucl. Instrum. Methods A **763**, 290 (2014).
 - [16] V. Abazov *et al.* (D0 Collab.), Phys. Rev. D **88**, 112002 (2013).
 - [17] V. Abazov *et al.* (D0 Collab.), Nucl. Instrum. Methods A **763**, 442 (2014).
 - [18] M. Mangano *et al.*, J. High Energy Phys. **07**, 001 (2003); M. Mangano, M. Moretti and R. Pittau, Nucl. Phys. B **632**, 343 (2002); F. Caravaglios *et al.*, Nucl. Phys. B **539**, 215 (1999).
 - [19] T. Sjöstrand *et al.*, Comput. Phys. Commun. **135**, 238 (2001).
 - [20] M. Czakon and A. Mitov, arXiv:1112.5675 (2011); M. Cacciari *et al.*, Phys. Lett. B **710**, 612 (2012); P. Baernreuther, M. Czakon and A. Mitov, Phys. Rev. Lett. **109**, 132001 (2012).
 - [21] R. Brun and F. Carminati, CERN Program Library Long Writeup W5013, 1993 (unpublished).
 - [22] V. Abazov *et al.* (D0 Collab.), Phys. Rev. Lett. **113**, 032002 (2014).
 - [23] S. Abachi *et al.* (D0 Collab.), Phys. Rev. Lett. **80**, 2063 (1998).
 - [24] V. Abazov *et al.* (D0 Collab.), Phys. Rev. D **80**, 092006 (2009).
 - [25] M. Bowler, Z. Phys C11, 169 (1981).
 - [26] Y. Peters, K. Hamacher, and D. Wicke, Fermilab-TM-2425-E (2006).
 - [27] P. Skands, Phys. Rev. D **82**, 074018 (2010); P. Skands, arXiv:1005.3457v4 (2011).
 - [28] S. Frixione *et al.*, J. High Energy Phys. **07**, 029 (2008); S. Frixione *et al.*, J. High Energy Phys. **03**, 092 (2006); S. Frixione and B. Webber, J. High Energy Phys. **06**, 029 (2002).
 - [29] G. Corcella *et al.*, J. High Energy Phys. **01**, 010 (2001).